Wireless Power Transfer, 2017, 4(1), 69–75. © Cambridge University Press, 2017
doi:10.1017/wpt.2017.3

RESEARCH ARTICLE

Adjusting the frequency of an autonomous push–pull converter for wireless power transfer through a voltage-controlled variable capacitor structure

JIANLONG TIAN[1] AND PATRICK HU[2]

This paper proposes a Voltage-controlled Variable Capacitor Structure (VVCS) to adjust the frequency of an autonomous push–pull converter. Unlike traditional switch mode capacitors or inductors where active switches are used, the equivalent capacitance of the VVCS varies with the on/off periods of a diode controlled by a DC voltage. The frequency of the autonomous push–pull converter can be controlled by this DC voltage when the VVCS is used as a variable resonant capacitor. As no active switching is involved in the VVCS, the circuit operates more smoothly than its switch mode counterpart so as to provide a simple way to adjust the operating frequency of the autonomous push–pull converter for high frequency and low electro magnetic interference operations. Mathematical model is developed for the relationship between the equivalent capacitance of the VVCS and the DC control voltage, and is verified by experimental results at more than 900 kHz with an approximately 12 W inductive power transfer system.

Keywords: Wireless power transfer, Inductive power transfer, Push–pull converter, Frequency control

Received 31 July 2016; Revised 9 January 2017; Accepted 13 January 2017; first published online 16 February 2017

I. INTRODUCTION

Wireless power transfer technology has been developing quickly and found many applications in areas such as moist harsh environments, charging the batteries of electric vehicles [1, 2], portable electronic devices [3, 4], and implanted electronic devices [5, 6], etc. Among a number of choices to transfer power wirelessly, inductive power transfer (IPT) is the most developed one so far. As there is usually a relatively large gap between the primary and secondary coils of an IPT system, its power transfer ability and efficiency are greatly limited compared with traditional tightly-coupled transformers and electric motors. To solve this problem, three major techniques are usually adopted, i.e. increasing the frequency of the system, improving the coupling degree between the primary and secondary coils, and taking advantage of the principles of resonance.

To maintain resonant operation for an IPT system and realize soft-switching, one method is to adjust the zero voltage switching (ZVS) frequency of the system dynamically to match the gate driving frequency. Traditionally, this is realized through switching mode capacitors [7–13] or inductors [14–22]. However, there are a few disadvantages with the conventional methods, such as complexity in circuit structure and control strategy, high electro magnetic interference (EMI), the frequency not being able to be adjusted smoothly, etc. A Balanced-voltage-controlled Variable Capacitor Structure has been proposed in the conference paper [23], but more detailed theoretical analysis and experimental results are necessary.

This paper proposes a Voltage-controlled Variable Capacitor Structure (VVCS) to adjust the ZVS frequency of an autonomous push–pull converter though a DC voltage. The DC voltage controls the conduction period of a diode in the VVCS. The equivalent capacitance of the VVCS changes with the variation of the conduction period of the diode. The basic operating principle of the method is explained in Section II of this paper. Section III presents theoretical modeling of the circuit. The experimental results are provided in Section IV. Finally Section V draws the conclusions.

II. THE PROPOSED METHOD AND BASIC OPERATING PRINCIPLE

Figure 1 shows the proposed VVCS applied to the resonant tank of an autonomous push–pull converter that has been introduced in section 7.3 of [24]. As can be seen, the common fixed value resonant capacitor in the resonant tank of the autonomous push–pull converter is replaced by the

[1]Electrical and Computer Engineering, University of Auckland, 368 Khyber Pass Road, Newmarket, Auckland 1023, New Zealand
[2]Electrical and Computer Engineering, University of Auckland, 38 Princes St, Auckland Central, Auckland, New Zealand
Corresponding author:
J. Tian
Email: jtia983@aucklanduni.ac.nz

VVCS as shown in the dashed block consisting of C_{up}, C_{dw}, D_c, and R_c. The equivalent capacitance C_e of the VVCS can be changed by the control voltage V_c. The higher V_c is, the larger the equivalent capacitance C_e, and the lower the ZVS frequency f_{zvs} of the converter.

The reason that the equivalent capacitance C_e can be controlled by the voltage V_c is that V_c influences the conduction period T_{con} of the diode D_c. The higher V_c is, the longer T_{con} is, because the higher V_c is, the larger the voltage on the anode of the diode D_c. When the diode conducts, C_{up} is shorted so that the equivalent capacitance of the VVCS is C_{dw}, while when the diode is off, the equivalent capacitance of the VVCS is C_{up} and C_{dw} in series. As the capacitance of C_{dw} is larger than that of C_{up} and C_{dw} in series, the longer the diode conducts, the larger the equivalent capacitance of the VVCS is.

III. THEORETICAL MODELING

The goal of the theoretical analysis is to find the relationship between the equivalent capacitance C_e of the VVCS and the control voltage V_c. For this purpose, the circuit in Fig. 1 is simplified as the ones shown in Fig. 2, which include only C_{up}, C_{dw}, D_c, R_c, and V_c of the original circuit and is driven periodically with positive and negative half cycle sinusoidal waves v_s in turn as being the same case as in the original circuit.

Figure 3 shows the typical waveforms of v_a, v_{ab}, the current i_D and i_{R_c} flowing through the diode D_c, and the resistor R_c, respectively, in steady state. The period when i_D is not zero represents the conduction period T_{con} of the diode D_c. It can be seen from Fig. 3 that the diode turns on when the voltage across it (v_{ab}) is zero and turns off when both the voltage across it (v_{ab}) and the current flowing through it (i_D) drops to zero. So the switching condition of the passive diode is very good, which helps to keep EMI low. This is achieved at the expense of higher power loss at the control resistor R_c. As can be seen from Fig. 3(d), a continuous current i_{R_c} flows through the resistor R_c. The value of i_{R_c} depends upon the values of R_c and the control voltage V_c. Smaller R_c and larger V_c lead to higher i_{R_c}. So within the control range, larger R_c and smaller V_c are preferred.

The major task of the theoretical analysis part is to derive the relationship between C_e and V_c, which is carried out in three steps. Firstly, the relationship between T_{con} and V_c is derived. Secondly, the relationship between C_e and T_{con} is found out. Finally, the relationship between C_e and V_c is calculated based on the above two relationships. To find out the relationship between T_{con} and V_c, two exact moments, i.e. the moment the diode starts to conduct- "t_{on}" and the moment the diode stops to conduct- "t_{off}" need to be determined first. After that, T_{con} can be calculated with (1):

$$T_{con} = t_{off} - t_{on}. \tag{1}$$

A. Determination of the moment the diode stops to conduct

Figure 4 shows the equivalent circuit of Fig. 2(b) when the diode is conducting. C_{up} and D_c are removed because an ideal conducting diode amounts to a short-circuit.

The diode is regarded as stopping to conduct when the current flowing through it (i_D) drops to zero, where i_D is governed by (2):

$$i_D = C_{dw}\frac{dv_s}{dt} + \frac{V_c}{R_c}. \tag{2}$$

Substitute $v_s = A_s \sin\omega t$ and $i_D = 0$ into (2), the moment the diode stops to conduct t_{off} can be derived as:

$$t_{off} = \frac{\arccos\left(-\dfrac{V_c}{\omega A_s R_c C_{dw}}\right)}{\omega}, \tag{3}$$

where A_s is the magnitude of the voltage of the resonant tank of the autonomous push–pull converter, which is roughly π times the voltage of the DC voltage source V_{DC} [24, 25].

According to simulation and the theoretical analysis result as shown in (3), the value of ωt_{off} varies between $\pi/2$ and π when the value of V_c varies between 0 and $\omega A_s R_c C_{dw}$.

B. Determination of the moment the diode starts to conduct

Figure 5 shows the equivalent circuit when the diode is not conducting, regarded as open so as to be removed from the circuit.

The voltage at the anode of the diode v_b is governed by (4):

$$\frac{dv_b}{dt} + \frac{1}{R_c(C_{up}+C_{dw})}\cdot v_b = \frac{\omega A_s R_c C_{dw}\cos\omega t + V_c}{R_c(C_{up}+C_{dw})}. \tag{4}$$

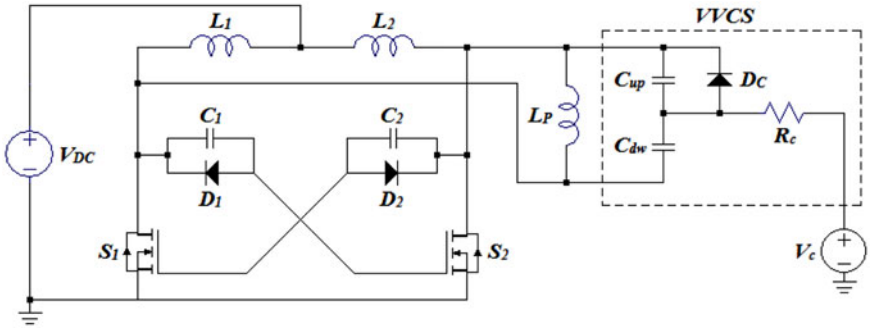

Fig. 1. The proposed VVCS applied to the autonomous push–pull converter.

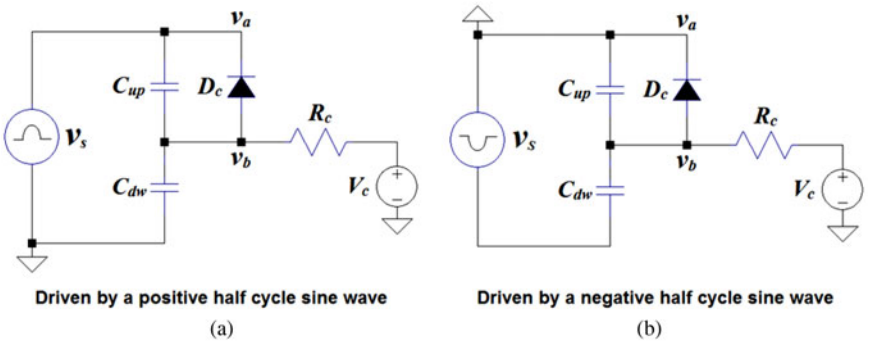

Fig. 2. The simplified circuit for theoretical analysis of the VVCS.

The solution of (4) is:

$$v_b = \omega k_1 \sin\omega t + k k_1 \cos\omega t + V_c + K e^{-kt}, \tag{5}$$

Where

$$k = \frac{1}{R_c(C_{up} + C_{dw})}, k_1 = \frac{\omega A_s C_{dw}}{(C_{up} + C_{dw})(\omega^2 + k^2)}.$$

The constant K in (5) can be determined by the initial condition, i.e. the value of v_b at the moment of t_2 (refer to Fig. 3). The moment t_2 can be expressed by (6):

$$t_2 = t_{off} - \frac{2\pi}{\omega}. \tag{6}$$

Substitute (3), (6) and $v_b = 0$ into (5), the constant K can be derived as:

$$K = \frac{-\omega k_1 \sqrt{1 - k_2^2} + k k_1 k_2 - V_c}{e^{-k \cdot \frac{\arccos(-k_2) - 2\pi}{\omega}}}, \tag{7}$$

where $k_2 = \frac{V_c}{\omega A_s R_c C_{dw}}$.

It can be seen from Fig. 3 that the diode starts to conduct when v_b becomes zero. Substituting $v_b = 0$ into (5) gives:

$$\omega k_1 \cdot \sin\omega t + k k_1 \cdot \cos\omega t + V_c + K e^{-kt} = 0. \tag{8}$$

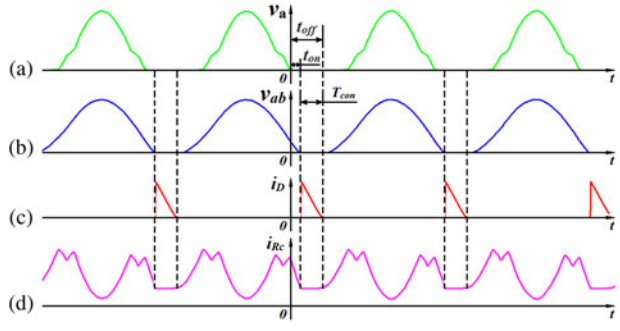

Fig. 3. Typical wave forms of the circuit: v_a, v_{ab}, i_D, and i_{R_c}.

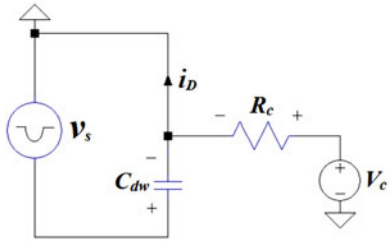

Fig. 4. The equivalent circuit when the diode is conducting.

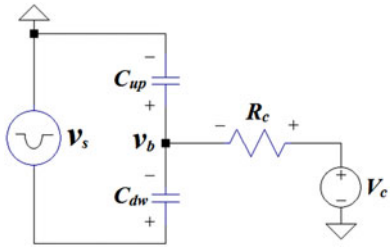

Fig. 5. The equivalent circuit when the diode is not conducting.

The exponential component Ke^{-kt} in (8) relates to the transient response of the circuit, which does not change much during a short time period of one or half a cycle of v_b, which is usually much smaller than the time constant τ of the circuit determined by the product of the capacitor and resistor $R_c(C_{up} + C_{dw})$. Consequently, Ke^{-kt} can be set roughly at a constant value Ke^{-kt_c}, where t_c can be simply zero. However, the closer t_c is to the moment the diode starts to conduct t_{on}, the smaller the error it causes.

From (8), the moment the diode starts to conduct can be derived as (9):

$$t_{on} \approx \frac{\arcsin\left(-\frac{V_c + K e^{-kt_c}}{k_1\sqrt{\omega^2 + k^2}}\right) - \arctan\frac{k}{\omega}}{\omega}. \tag{9}$$

The value of ωt_{on} varies between 0 and $\pi/2$, which is in consistent with what has been observed from a wide range of simulation studies.

C. The relationship between T_{con} and V_c

Substitute (3) and (9) into (1), the conduction period T_{con} of the diode can be derived as:

$$T_{con} \approx \frac{\arccos\left(-\frac{V_c}{\omega A_s R_c C_{dw}}\right) + \arcsin\left(\frac{V_c + Ke^{-kt_c}}{k_1\sqrt{\omega^2 + k^2}}\right) + \arctan\frac{k}{\omega}}{\omega}. \tag{10}$$

When the circuit quality factor Q is high, the angular frequency ω in (10) can be simplified as the undamped natural oscillation frequency as expressed by (11):

$$\omega = 2\pi f = \frac{1}{\sqrt{LC}}. \tag{11}$$

Substitute (11) into (10) gives (12),

$$T_{con} = \sqrt{LC_{on}} \cdot \left(\arccos\left(-\frac{V_c \cdot \sqrt{LC_{on}}}{A_s R_c C_{dw}}\right) - \arcsin\left(-\frac{V_c + Ke^{-kt_c}}{k_1\sqrt{\frac{1}{LC_{off}} + k^2}}\right) + \arctan(k\sqrt{LC_{off}})\right) \tag{12}$$

where C_{on} and C_{off} represent the capacitance of the circuit when the diode is on and off, respectively, as expressed by (13) and (14):

$$C_{on} = C_{dw}, \tag{13}$$

$$C_{off} = \frac{C_{up}C_{dw}}{C_{up} + C_{dw}}. \tag{14}$$

D. The relationship between C_e and V_c

To find the relationship between C_e and V_c, the relationship between C_e and T_{con} needs to be found first, which can then be combined with (12) to get the relationship between C_e and V_c. Derivation of the relationship between C_e and T_{con} is based on a LC parallel resonance circuit. The frequency of such a circuit is governed by (11). From (11), the equivalent capacitance of the circuit can be derived as:

$$C_e = \frac{1}{L \cdot (2\pi f)^2} = \frac{T^2}{4\pi^2 L}, \tag{15}$$

where T represents the period of one cycle, i.e. the reciprocal of the frequency "f". Suppose that the inductance of the parallel LC resonance circuit is fixed while the capacitance of the parallel LC resonance circuit switches between two distinct values C_{on} and C_{off} periodically and their duration are t_{on} and t_{off}, respectively. According to (15), the equivalent capacitance C_e of the circuit is:

$$C_e = \frac{(t_{on} + t_{off})^2}{4\pi^2 L}. \tag{16}$$

Actually t_{on} equals T_{con}, and t_{off} can be derived based on the principle that the wave forms when the capacitance is C_{on} and C_{off}, respectively, need to go continuously into each other. Finally the relationship between C_e and T_{con} is derived as (17):

$$C_e = \frac{\left(2\pi\sqrt{LC_{off}} + \left(1 - \sqrt{\frac{C_{off}}{C_{on}}}\right) \cdot T_{con}\right)^2}{4\pi^2 L}. \tag{17}$$

Substituting (12) into (17) gives the relationship between C_e and V_c as expressed by (18):

$$C_e = \left[\sqrt{C_{off}} + \frac{\sqrt{C_{on}} - \sqrt{C_{off}}}{2\pi}\left(\arccos\left(-\frac{V_c\sqrt{LC_{on}}}{A_s R_c C_{dw}}\right) - \arcsin\left(-\frac{V_c + Ke^{-kt_c}}{k_1\sqrt{\frac{1}{LC_{off}} + k^2}}\right) + \arctan(k\sqrt{LC_{off}})\right)\right]^2. \tag{18}$$

Equation (18) can be simplified as (19):

$$C_e = \left[\sqrt{C_{off}} + \frac{\sqrt{C_{on}} - \sqrt{C_{off}}}{2\pi} \cdot T_{rad}\right]^2, \tag{19}$$

where:

$$T_{rad} = \arccos\left(-\frac{V_c\sqrt{LC_{on}}}{A_s R_c C_{dw}}\right) - \arcsin\left(-\frac{V_c + Ke^{-kt_c}}{k_1\sqrt{\frac{1}{LC_{off}} + k^2}}\right) + \arctan(k\sqrt{LC_{off}}). \tag{20}$$

Actually, T_{rad} is the diode conduction period T_{con} in radians. Theoretically, T_{rad} changes from 0 to 2π. When T_{rad} is 0, (19) becomes:

$$C_e = C_{off}. \tag{21}$$

It means that when the diode conduction period is 0, the equivalent capacitance is C_{off}, which coincides exactly with the real circuit situation. While when T_{rad} is 2π (meaning that the diode always conducts so as to be equivalent to a short-circuit), (19) becomes:

$$C_e = C_{on}. \tag{22}$$

Again, this is in agreement with the basic concept and practical circuit situation.

It can be seen from (21) and (22) that theoretically the equivalent capacitance of the VVCS changes between C_{on}

and C_{off}, which correspond to C_{dw} and the capacitance of C_{up} and C_{dw} in series, respectively, as can be seen from (13) and (14). So the variation range of the equivalent capacitance of the VVCS is determined by the values of the two capacitors C_{up} and C_{dw}. When the value of C_{dw} is fixed, a smaller C_{up} results in a larger the variation range of the VVCS. When the values of C_{up} and C_{dw} are fixed, a smaller value of R_c leads to larger adjustable range of the VVCS with the same variation range of the control voltage V_c.

E. The relationship between f_{zvs} and V_c

Substituting (18) into (11) gives the relationship between f_{zvs} and V_c as expressed by (23). Figure 8 in Section IV shows the theoretical relationship between the ZVS frequency f_{zvs} and the control voltage V_c got from (23) using parameters as shown in Table 1 of Section IV together with the experimental results, from which it can be seen that the theoretical and experimental results agree with each other quite well.

$$f_{zvs} = \frac{1}{2\pi\sqrt{L}\cdot\left(\sqrt{C_{off}} + \frac{\sqrt{C_{on}}-\sqrt{C_{off}}}{2\pi}\left(\arccos\left(-\frac{V_c\sqrt{LC_{on}}}{A_s R_c C_{dw}}\right)\right.\right.} \\ \left.\left. - \arcsin\left(-\frac{V_c + Ke^{-kt_c}}{k_1\sqrt{\frac{1}{LC_{off}}+k^2}}\right) + \arctan\left(k\sqrt{LC_{off}}\right)\right)\right). \tag{23}$$

IV. EXPERIMENTAL RESULTS

Figure 6 shows the experimental setup, which includes the push–pull converter and the VVCS (refer to Fig. 1), the primary and secondary side coils L_P and L_S, and the parallel tuning, full-bridge regulation pick-up circuit. Table 1 shows the components and parameters of the primary and secondary side circuits, where C_s is the parallel tuning capacitor of the pick-up circuit, $D_{s_1} \sim D_{s_4}$ the regulation diodes, C_f the filter capacitor, and R_{load} the load resistance.

Figure 7 shows the experimental and theoretical relationships between the operating frequency of the converter and the control voltage V_c together under two different situations, i.e. when there is ($R_{load} = 100\ \Omega$) and there is no load, from which it can be seen that the theoretical and experimental results agree with each other quite well. It shows that the operating frequency is negatively related to the control voltage V_c because the higher V_c is, the larger the equivalent capacitance of the VVCS as explained in Sections II and III.

Table 1. Parameters and components of the primary and secondary side circuits.

V_{DC} (V)	L_1, L_2 (mH)	C_1, C_2 (nF)	D_1, D_2	S_1, S_2
12	1	4.5	BYV26C	IRFP240
C_{up} (nF)	C_{dw} (nF)	D_c	L_P (μH)	k
1	20	C3D02060F	8.5	0.7
L_S (μH)	C_S (nF)	$D_{S_1} \sim D_{S_4}$	C_f (μF)	R_{load} (Ω)
8.3	4	PMEG10020AELRX	10	100

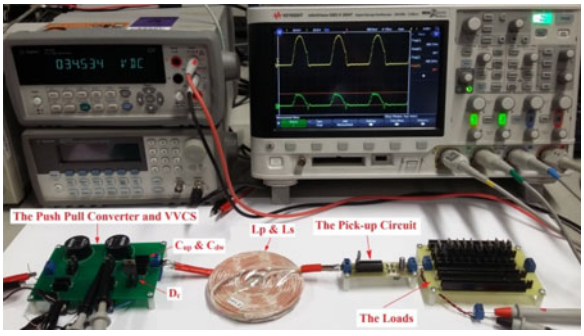

Fig. 6. The experimental setup.

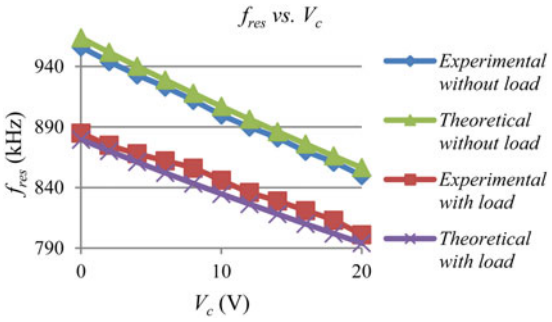

Fig. 7. Experimental and theoretical relationships between the frequency of the converter and the control voltage.

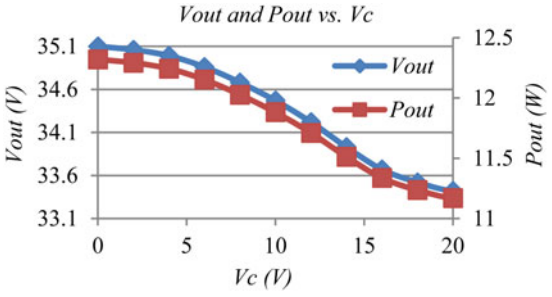

Fig. 8. Experimental relationships of the output voltage V_{out} and power P_{out} against the control voltage V_c.

Figure 8 shows the experimental relationships of the output voltage V_{out} and power P_{out} against the control voltage V_c when the load resistance R_{load} is 100 Ω. As the circuit is designed to resonant when the control voltage is zero, the output voltage decreases with the increase of the control voltage because the higher the control voltage is, the larger the equivalent capacitance of the VVCS and therefore the lower the frequency of the converter becomes, so that the operating frequency deviates from the resonant frequency further.

Figure. 9 shows the relationship between the load resistance R_{load} and the output power P_{out} when the control voltage V_c is zero, from which it can be seen that the output power changes with the change of the load resistance, and reaches the maximum power of about 12 W when the load resistance is 100 Ω.

Figure 10 shows the experimental waveforms of v_a, v_{ab}, the current i_D, and i_{R_c} flowing through the diode D_c and the resistor R_c, respectively, from which it can be seen that a short

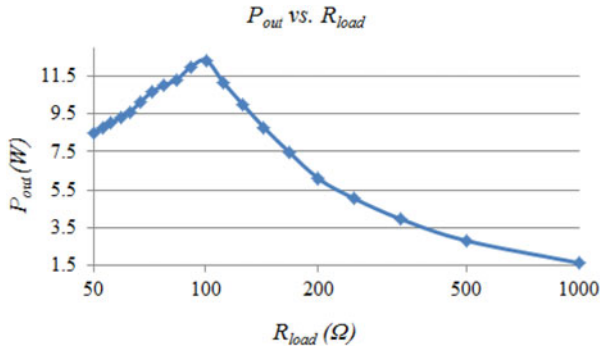

Fig. 9. Experimental relationship between the output power P_{out} and the load resistance R_{load}.

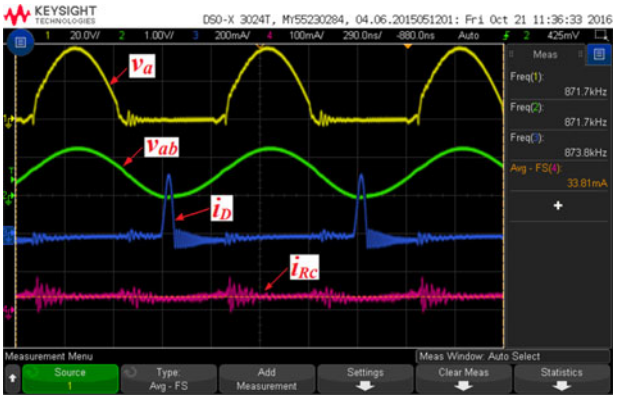

Fig. 10. Experimental waveforms of v_a, v_{ab} and the current i_D and i_{R_c} flowing through D_c and R_c.

period transition from on to off of the diode D_c causes negligible distortion in its voltage (v_{ab}) because of the favorable switching conditions of the diode.

V. CONCLUSIONS

This paper proposes a new method to adjust the ZVS frequency of an autonomous push–pull converter by replacing the common fixed value resonant capacitor in the resonant tank with a VVCS. The equivalent capacitance of the VVCS can be adjusted simply with a DC voltage, which influences the ZVS frequency, and therefore the output voltage and power of the IPT system. As a passive diode instead of an active switch is used to control the conduction time of a capacitor in the VVCS, the equivalent capacitance of the VVCS can be adjusted more smoothly with less EMI than traditional switch mode capacitors. Mathematical models for the relationship between the equivalent capacitance of the VVCS and the frequency of the converter against the control voltage is developed, and practical experiments are carried out to prove their validity.

REFERENCES

[1] Covic, G.A.; Boys, J.T.; Tam, A.M.W.; Peng, J.C.H.: Self tuning pick-ups for inductive power transfer, in IEEE Power Electronics Specialists Conf., 2008. PESC 2008, 2008, 3489–3494.

[2] James, J.; Boys, J.; Covic, G.: A variable inductor based tuning method for ICPT pickups, in The 7th Int. Power Engineering Conf., 2005. IPEC 2005, 2005, **2**, 1142–1146.

[3] Si, P.; Hu, A.P.; Malpas, S.; Budgett, D.: Switching frequency analysis of dynamically detuned ICPT power pick-ups, in Int. Conf. on Power System Technology, 2006. PowerCon 2006, 2006, 1–8.

[4] Hsu, J.U.W.; Hu, A.P.: Determining the variable inductance range for an LCL wireless power pick-up, in IEEE Conf. on Electron Devices and Solid-State Circuits, 2007. EDSSC 2007, 2007, 489–492.

[5] Si, P.; Hu, A.P.; Malpas, S.; Budgett, D.: A frequency control method for regulating wireless power to implantable devices, IEEE Trans. Biomed. Circuits Syst, 2008, **2**, 22–29.

[6] Hamill, D.C.; Bina, M.T.: The bootstrap variable inductance and its applications in AC power systems, in 14th Annual Applied Power Electronics Conf. and Exposition. APEC '99, 1999, **2**, 896–902.

[7] Al-Kuran, S.: GaAs switched capacitor voltage converter, in WESCON/96, 1996, 130–134.

[8] Wong, C.S.; Loo, K.H.; Lai, Y.M.; Chow, M.H.L.; Tse, C.K.: Accurate capacitive current balancing in multistring LED lighting systems based on switched-capacitor-controlled LCC resonant network. IEEE Trans. Power Electron., **PP** (2016), 1.

[9] Gu, W.-J.; Harada, K.: A new method to regulate resonant converters. IEEE Trans. Power Electron., **3** (1988), 430–439.

[10] Gu, W.-J.; Harada, K.: A circuit model for the class E resonant DC-DC converter regulated at a fixed switching frequency. IEEE Trans. Power Electron., **7** (1992), 99–110.

[11] Harada, K.; Gu, W.-J.: Steady state analysis of Class E resonant DC-DC converter regulated under fixed switching frequency, 19th Annual IEEE *in* Power Electron. Specialists Conf. PESC'88 Record, 1988, 3–8.

[12] Harada, K.; Gu, W.J.; Murata, K.: Controlled resonant converters with switching frequency fixed, IEEE *in* Power Electronics Specialists Conf., 1987, 431–438.

[13] Perez-Nicoli, P.; Castro, P.; Silveira, F.: A series-parallel switched capacitor step-up DC-DC converter and its gate-control circuits for over the supply rail switches, in 2014 IEEE 5th Latin American Symp. on Circuits and Systems (LASCAS), 2014, 1–4.

[14] Aghdam, S.R.; Babaei, E.; Zadeh, S.G.: Improvement the performance of switched-inductor Z-source inverter, in Industrial Electronics Society, IECON 2013 – IEEE 39th Annual Conf., 2013, 876–881.

[15] Fang Lin, L.; Hong, Y.: Switched inductor two-quadrant DC/DC converter with fuzzy logic control, in Proc. of the IEEE 1999 Int. Conf. on Power Electronics and Drive Systems. PEDS '99, 1999, **2**, 773–778.

[16] Hu, Y.; Li, K.; Yin, Z., Ioinovici, A.: Switched-inductor-based non-isolated large conversion ratio, low components count DC-DC regulators, in 2015 IEEE Energy Conversion Congress and Exposition (ECCE), 2015, 1398–1405.

[17] Ismeil, M.A.; Kouzou, A.; Kennel, R.; Ibrahim, A.A.; Orabi, M., Ahmed, M.E.: Modeling of non-ideal improved Switched Inductor (SL) Z-source inverter, in Int. Aegean Conf. on Electrical Machines and Power Electronics and Electromotion, Joint Conf., 2011, 472–477.

[18] Kossel, M.; Morf, T.; Buchmann, P.; Schmatz, M.L.; Menolfi, C.; Toifl, T.: Switched Inductor with wide tuning range and small inductance step sizes. IEEE Microw. Wireless Compon. Lett., **19** (2009), 515–517.

[19] Liu, H.; Li, F.: A novel high step-up converter with a quasi-active switched-inductor structure for renewable energy systems. IEEE Trans. Power Electron., **31** (2016), 5030–5039.

[20] Mousa, M.; Ahmed, M.E.; Orabi, M.: New converter circuitry for high v applications using switched inductor multilevel converter, in 2011 IEEE 33rd Int. Telecommunications Energy Conf. (INTELEC), 2011, 1–8.

[21] Nguyen, M.K.; Le, T.V.; Park, S.J.; Lim, Y.C.; Yoo, J.Y.: Class of high boost inverters based on switched-inductor structure. IET Power Electron., **8** (2015), 750–759.

[22] Tang, Y.; Fu, D.; Wang, T.; Xu, Z.: Hybrid switched-inductor converters for high step-up conversion. IEEE Trans. Ind. Electron., **62** (2015), 1480–1490.

[23] Tian, J., Hu, A.P.: Adjusting the frequency of an autonomous push pull converter for wireless power transfer by varying the equivalent resonant capacitance through balanced DC voltage control, in 2015 IEEE PELS Workshop on Emerging Technologies: Wireless Power (WoW), 2015, 1–4.

[24] Hu, A.P.: Selected resonant converters for IPT power supplies. PhD thesis, The University of Auckland, ResearchSpace@ Auckland, 2001.

[25] Si, P.; Hu, A.P.; Budgett, D.; Malpas, S.; Yang, J.; Gao, J.: Stabilizing the operating frequency of a resonant converter for wireless power transfer to implantable biomedical sensors, in Proc. 1st Int. Conf. Sensing Technology, 2005, 477–482.

Jianlong Tian received his B.S. degree in Mechanical and Electric Engineering from the Agricultural University of Hebei, Baoding, China, in 1989; and his M.S. degree in Detection Technology and Automatic Equipment from the Beijing University of Chemical Technology, Beijing, China, in 2003. He has been working towards his Ph.D. degree at the University of Auckland, Auckland, New Zealand, since 2012. For more than eight years he worked as an Electronic Engineer for a couple of companies in Beijing, China. His current research interest include the high frequency and resonant operation of IPT systems, voltage controlled variable capacitors and soft-switching DC-AC power converters.

Dr. Aiguo Patrick Hu received his B.S. and M.S. degrees from Xian Jiaotong University, Xian, China, in 1985 and 1988, respectively; and his Ph.D. degree from the University of Auckland, Auckland, New Zealand, in 2001. He served as a Lecturer and as a Director of the China Italy Cooperative Technical Training Center in Xian, China, and as the General Manager of a technical development company. He stayed for a semester at the National University of Singapore (NUS), Singapore, as an Exchange Postdoctoral Research Fellow with funding from the Asian2000 Foundation. Patrick is a leading researcher in the field of wireless power technologies. He holds 15 patents in wireless/contactless power transfer and microcomputer control technologies, has published papers in more than 200 peer reviewed journal and conference proceedings and has over 2600 citations. He authored the first monograph on wireless inductive power transfer technology, and contributed 4 book chapters on inductive power transfer modeling/control as well as electrical machines. Patrick is currently with the Department of Electrical and Electronic Engineering, University of Auckland, Auckland, New Zealand. He is also the Head of Research of PowerbyProxi Ltd, as well as a Guest Professor of Chongqing University, Chongqing, China, and Taiyuan University of Technology, Taiyuan, China. He is a Senior Member of IEEE, a former Chairman of IEEE NZ Power Systems/Power Electronics Chapter, and the current Chairman of the NZ North Section. He served as Secretary/Treasurer of the NZ Chinese Scientists Association, and is now the Vice President. His current research interests include wireless/contactless power transfer systems, and the application of power electronics in renewable energy systems.